Experimental observation of the quasiperiodic modes in a rotating Couette system

Y. Takeda and W. E. Fischer
Paul Scherrer Institute, CH-5232 Villigen PSI, Switzerland

J. Sakakibara and K. Ohmura
Department of Mechanical Engineering, Keio University, 3-14-1 Hiyoshi, Kohoku-ku 223, Yokohama, Japan
(Received 21 September 1992)

We experimentally observed the spatiotemporal velocity field of modulated waves (quasiperiodic mode) in a Couette-Taylor system for Reynolds number $9 \leq R/R_c \leq 28$. A power spectrum averaged over four axial wavelengths showed clear evidence of the coexistence of two quasiperiodic modes for a wide range of Reynolds number and the first azimuthal wave mode disappeared at $R/R_c \approx 18$.

PACS number(s): 47.20.−k, 47.32.−y

I. INTRODUCTION

Flow in a rotating Couette system is frequently used to investigate a passage of flow transition from laminar to turbulence through chaos because the transition is gradual. In a system with the outer cylinder fixed, the fluid occupying the annular gap moves as a sheet without an axial velocity component for small Reynolds numbers. The first flow instability sets in at a critical Reynolds number (R_c) to form a roll structure [Taylor vortex flow (TVF)] with a nonzero axial velocity component. At higher Reynolds numbers (depending on the radius ratio) a second instability sets in and an azimuthal wave appears [wavy vortex flow (WVF)]. Power-spectrum studies [1] and numerical simulations [2] have indicated that this wavy vortex flow has a single wavy mode (wave mode m_1 or m_w) and a motion which is periodic. At still higher Reynolds numbers, this azimuthal wave is modulated by a second wave mode [modulated wavy vortex flow (MWV)] (wave mode m_2) and the motion becomes quasiperiodic.

The characteristics of this quasiperiodic mode have not yet been well understood. On this quasiperiodic flow, Gorman and Swinney (GS) [3] found experimentally that the m_2 wave extends over the roll and modulates the m_1 mode, leading to a spatial flattening of the WVF. On the other hand, Zhang and Swinney (ZS) [4] found another type of m_2 mode that appears mainly near the outflow region with a higher phase speed, inducing in addition the appearance of a ripple on the roll.

In numerical analysis, Coughlin and Marcus [5] succeeded in simulating the MWV flow with a GS mode and also showed the characteristics of the ZS mode. Recently, Coughlin *et al.* [6] found that these two quasiperiodic modes (GS and ZS modes) can coexist over some range of the Reynolds number. They also reported the experimental verification of this coexistence for a very limited range of the Reynolds number. The multiplicity of the quasiperiodic wavy modes is of importance to the transition to chaos and finally to turbulence. However, since these three modes have similar spatial characteristics in the axial direction and temporally in a fixed laboratory frame, a well-resolved power-spectrum analysis is believed to be indispensable. This is presently not available through numerical simulations. In this report, we present our recent experimental results on this quasiperiodic mode, especially on the coexistence of the GS and ZS modes, and, moreover, show that at a higher R, the first azimuthal mode (WVF) decays and only m_2 modes remain.

II. EXPERIMENT

Our Couette system (Fig. 1) has a radius ratio $\eta = R_i/R_o = 0.904$ (R_i is the radius of inner cylinder, 94.0 cm, and R_o that of outer cylinder, 104.0 cm) and an aspect ratio $\Gamma = L/d = 20$ ($d = R_o - R_i$, L is the column length). Only the inner cylinder is rotated, with the end boundaries fixed to the outer cylinder, which is at rest. The Reynolds number R is defined as $R = \Omega R_i d/\nu$ (Ω is

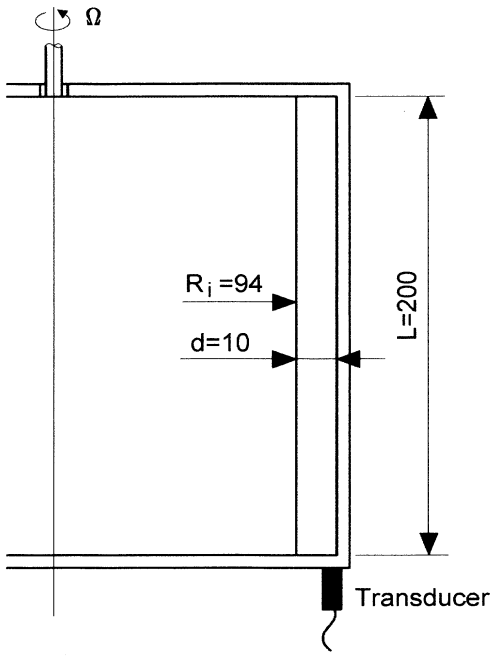

FIG. 1. Schematic of the experimental setup.

rotational speed, ν is kinematic viscosity) and the reduced Reynolds number as $R^*=R/R_c$. In the present configuration, the critical Reynolds number R_c for the onset of TVF is 134.7 [7]. The liquid used in this experiment was a mixture of water and 30% glycerol. The measuring method is by ultrasound velocity profile (UVP) monitor, which can successively obtain a series of instantaneous velocity profiles. The transducer was set onto the outer surface of one of the stationary end walls and is perpendicular to it with its center at the inner wall of the outer cylinder. The ultrasound beam diameter is 5 mm. This setup measures the velocity profile of the axial velocity component as a function of axial position, namely, $V_z(z,t)$ at the outer wall position. Thus the measurement volume is one-half of a disk shape of radius 2.5 mm and thickness 0.75 mm. The measurement of the velocity profile was focused on the spatial range from 40 to 135 mm with 128 spatial points in order to eliminate the end-wall effect. This setup of the UVP monitor required a measuring time of 72–130 msec for a velocity level of a few mm/sec (including data transfer). The 1024 successive profiles were recorded. More details of the measuring method and the experimental system are described in Refs. [8,9]. The present UVP system has been improved in comparison to the previous model. The spatial resolution has been halved, measuring time decreased by a third, and the sampling speed reduced to $\frac{1}{6}-\frac{1}{10}$.

The experimental procedure was as follows. First, the inner cylinder was rotated up to a very high R^* number and then slowly reduced to the preset R^* number, which was roughly $R^*\approx 15$ for most cases. We concentrated our measurements only on the axial wave state of eight roll pairs, and when a different axial wave state appeared the run was started again from the beginning. When an eight-roll-pair state was generated, the system was left for approximately 1.5 h to allow for decay of the flow noise. This waiting time corresponds to a relaxation time reported by Snyder [10] and is very conservative compared to our earlier experience [11]. When a measurement was started, it took roughly 2.5 min to record 1024 velocity profiles. Then the Reynolds number was reduced by approximately $\Delta R^*=0.2-0.7$ and the next measurement was made after roughly 15–20 min of waiting time. Once an R^* value of roughly 9 was reached and prior to the disappearance of the WVF, the rotation was increased with the same increments of R^* up to 30. This ensured that a targeted axial and first azimuthal wave state was maintained for a series of measurements.

III. RESULTS AND DISCUSSION

A data set obtained by UVP is composed of velocity values at 128 positions in space and 1024 in time. Power spectra were computed using fast Fourier transform for all spatial positions, generating 128 power spectra at 512 frequencies. This is a space-dependent power spectrum $P(z,f)$, from which a spatial distribution of power at each frequency can be obtained [9]. This power spectrum is then averaged over the spatial range from 40 to 120 mm (ca. four axial wave lengths) to give a space-averaged power spectrum.

Figure 2 shows examples of the space-averaged power spectra computed as above for different R^* numbers. Since they are averaged over the space, a very clear peak structure is revealed; much cleaner than the one usually obtained by pointwise measurements [3,6]. This makes peak identification very easy and definitive. An example is given in Table I. Frequency resolution is 7.4 mHz and the peak identification for harmonics and their linear combination was made based on an accuracy of ± 1 unit of this resolution. This identification criterion was used for all the data sets given in this report.

Figure 2(a) shows a WVF mode at $R^*=9.05$, where a single component f_W is seen with its higher harmonics. Background level is low. Figure 2(b) shows the MWV mode at $R^*=14.08$. In this spectrum, f_W from the WVF mode has the largest power and its higher harmonics can be seen up to $3f_W$. The second largest peak (labeled 7), however, is not a second mode. Using this peak as the MWV mode failed to identify most of the peaks as its linear combination with f_W. For successful identification it was necessary to take two peaks, labeled f_G and f_Z, as the fundamental second modes. Most of the other prominent peaks in the spectrum could then be identified as linear combinations of f_W and f_G or f_Z in this spectrum (see Table I). It is noteworthy to state that we found no combination between f_G and f_Z except for the one labeled 10. The background level is as low as shown in Fig. 2(a). Figure 2(c) is a spectrum at $R^*=21.27$. Here again we identified only two fundamental modes (f_G and f_Z) from which most other peaks could be assigned by their linear combinations. In this

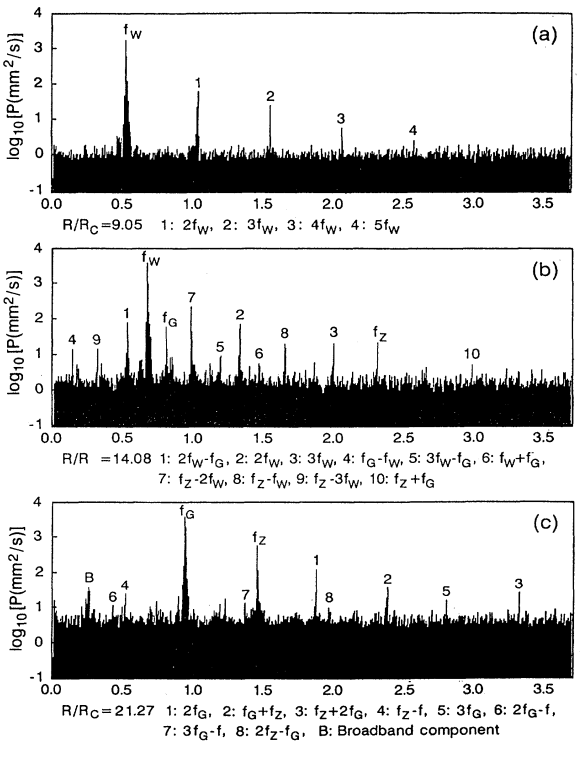

FIG. 2. Space-averaged power spectra for (a) $R^*=9.05$, (b) $R^*=14.08$, and (c) $R^*=21.27$.

TABLE I. An example of the peak identification for the spectrum of Fig. 2(b), in the order of peak power. The frequency resolution is 3.5 mHz.

No.	Frequency (Hz)	Identified as	Marked in Fig. 2(b)
1	0.6640	WVF	f_W
2	0.9816	ZS-2WVF	7
3	0.5269	2WVF-GS	1
4	1.3353	2WVF	2
5	0.8012	GS	f_G
6	2.3169	ZS	f_Z
7	1.6457	ZS-WVF	8
8	1.9993	3WVF	3
9	0.3176	ZS-3WVF	9
10	0.1371	GS-WVF	4
11	1.1982	3WVF-GS	5
12	1.4652	WVF-GS	6
13	2.9809	GS+ZS	10

spectrum, we see a broad peak (labeled B). By looking at the spatial (axial) distribution of the power (as discussed in [9]), one can identify it as a so-called broadband component of the MWV. This is still narrower compared with the ones reported earlier [1]. Here the background level is roughly five times higher.

In these spectra, we identified one, two, and three fundamental modes, depending on R^*. We will discuss why these three modes are intrinsic to the WVF and the MWV. The frequencies of peaks identified as fundamental modes are normalized by the rotational speed and plotted with respect to R^* in Fig. 3. This figure clearly shows that these three modes form three distinct curves. One can easily deduce that the middle curve corresponds to the WVF because it is the only one which exists at a value of R^* smaller than 12. What is plotted in this figure is the product of the wave-mode number m and its phase speed c. Since our measurement was fixed at one angular position, it is not possible to identify its wave state m directly from our data. However, by using an empirical rule on the phase speeds [12] for the GS mode, $c_2/c_1 \approx \frac{4}{3}$ and the ZS mode $c_2/c_1 \approx 2$, and assuming for the WVF mode a phase speed of 0.33 (this value is for $\eta = 0.875$), and it can be slightly different for our radius ratio [13]), we can obtain integer wave-mode numbers for each component as $m_W = 7$, $m_G = m_Z = 4$ (Table II). At the same time the top curve was assigned as the ZS mode and the bottom one as the GS mode.

A distinction of these fundamental modes and their assignment to different wave modes can be ascertained by observing the raw velocity distributions. Figure 4 shows examples of instantaneous velocity distributions for $R^* = 10.6$ and 14.7. Since we have a series of such velocity profiles, we can review the data set serially on a computer screen as a movie. As we measure the axial component of velocity, we clearly observe four roll pairs. As seen serially, the profile moves to the right and to the left, showing a single periodic oscillation for the WVF ($R^* = 10.6$) and a doubly periodic oscillation for the WVF and GS mode ($R^* = 14.7$). An interesting observation for $R^* = 14.7$ is a ripple on the shoulder of each roll. It was also observed that this ripple appears more strongly at the outflow region but moves around within a roll. Such a ripple is not observed for $R^* = 10.6$. Hence, this wave appearing as a ripple in the velocity distribution might correspond to the ZS mode.

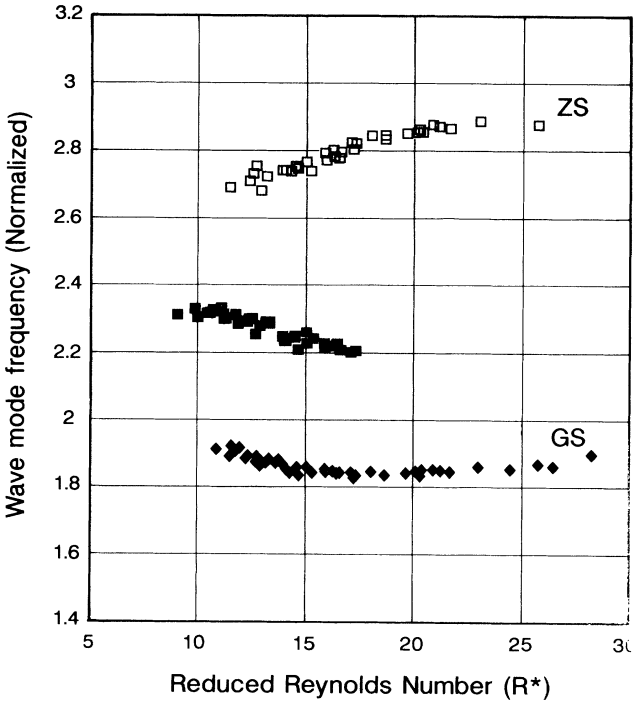

FIG. 3. Normalized wave frequencies of the intrinsic modes vs Reynolds number.

The spatial distribution of power for each fundamental mode are given in Fig. 5 together with a time-averaged velocity profile in order to show the average position of the roll's inflow and outflow. As we discussed in detail in [9], the WVF mode has a larger power equally at the inflow and outflow region, while the GS mode has narrower distribution at the outflow. A ZS mode [Fig. 5(d)] here, however, shows clearly a quite different spatial distribution from the other two [Figs. 5(b) and 5(c)]. The distribution is slightly broad but intensified in one roll of a pair, with the power largest near the center of that roll.

TABLE II. Estimates of the m values. The average is for the whole data set. $c_1 = 0.33$. GS and ZS are computed by (Average)$/c_2$, where $c_2/c_1 = 1.42$ for GS and 2.12 for ZS. These ratios are slightly different from the ones given in the text so that all mode numbers are integers.

	f_1/Ω	f_2/Ω	f_3/Ω
Average	2.275±0.0418	2.795±0.0590	1.857±0.0249
(Average)$/c_1$	**6.894**	8.469	5.656
GS	4.841	5.964	**3.985**
ZS	3.250	**3.995**	2.669
Mode number m	7	4	4

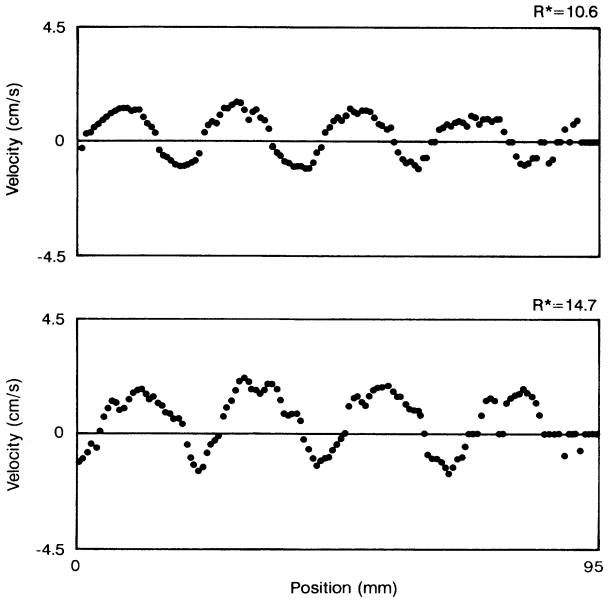

FIG. 4. Examples of an instantaneous velocity profile. $R^*=10.6$ and 14.7. The position starts 40 mm from one end. Distance between two points is 0.75 mm.

This result is not contrary to the original observation by Zhang and Swinney [4]. They reported, "... these modes were observable at all positions (except at a vortex inflow boundary). The intensity was greatest near the center of the vortices." In summary, the three modes given here are distinct and intrinsic; they are the WVF mode, the GS mode, and the ZS mode, respectively.

It is shown in Fig. 3 that the WVF mode appears at $R^*\approx 9$. This agrees well with earlier observations [14]. Since our intention was not to determine a critical value, which is known to depend on the radius ratio and wave state m_W, this R^* value is merely an indication of its appearance. At around $R^*\approx 12$, both the GS mode and the ZS mode appear. The GS mode seems to appear at slightly lower R^* than for the ZS mode. For higher Reynolds numbers three modes of WVF, GS, and ZS modes coexist until the WVF mode disappears at $R^*\approx 18$. The disappearance of the WVF mode was also seen by Gorman and Swinney [14] and was identified by the disappearance of the azimuthal wavy structure and flattening of each roll with smaller structure within the roll. For this range of R^* ($12<R^*<18$) each wave-mode frequency (equivalent to the phase speeds) varies by about 10%, but the tendency is different. That is, the WVF shows a decrease. It also shows a decrease for the GS mode but then stays constant for $R^*>15$. On the other hand, the ZS mode shows an increase until $R^*\sim 21$ and then stays constant. The reason for such variation of phase speed versus R has not been studied so far. Even after disappearance of the WVF at $R^*\sim 18$, the GS and ZS modes can still coexist, but the GS mode seems more stable with respect to the change of Reynolds number because we observed only a GS mode in some of our data obtained at higher R^*. Coughlin and Marcus [5] argued that the ZS mode is more stable for lower R and the GS mode for

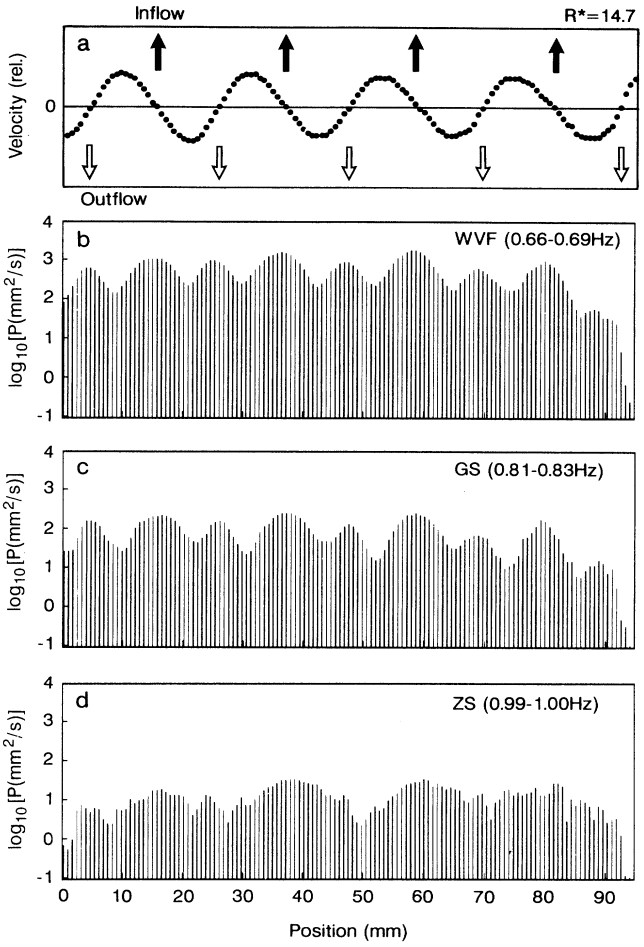

FIG. 5. Spatial distributions of power for different wave modes. $R^*=14.7$. (a) Time-averaged velocity profiles. Positions of inflow and outflow are marked. Spatial distributions for frequencies of (b) 0.66–0.69 Hz, (c) 0.18–0.83 Hz, and (d) 0.99–1.00 Hz.

higher R in terms of growth rate. This is in general agreement with our result, although our waiting time after the change of R is of the order of 10 min. In their simulation, the range where two modes coexist is very narrow ($9.0<R^*<9.6$) whereas in our observation it is much wider, most likely $12\le R^*<23$–26. We believe the main reason for this discrepancy is that the measurement volume in our experiment is relatively large and the evaluation was made for a wide spatial area defined by an average over four axial wavelengths, while others are by pointwise measurement and thus local. For these variations, we found no hysteresis. Curves for the data with increasing R and decreasing R collapsed onto the same lines and showed exactly the same characteristics.

IV. CONCLUDING REMARKS

In conclusion, we have observed the quasiperiodic mode in a rotating Couette system and found that both the GS and the ZS modes coexist (in addition to the WVF mode) for a relatively wide range of Reynolds number.

However, they have different characteristics as far as the spatial distribution of their power. The GS mode has a larger power at the vortex boundaries whereas the ZS mode is broadly distributed, being more intense near the vortex center. We also found that by increasing the Reynolds number the WVF mode disappears first among those three modes and afterwards there remain two modes of the GS and the ZS modes. However, the ZS mode seems less stable at still higher Reynolds numbers, which suggests that the GS mode is the spatial mode observed in the turbulent regime [7]. At this point, a question can be raised. For the R^* range where the three modes coexist, why is the interaction between the GS and the ZS modes hardly observed and how relevant is the coexistence of these modes to chaos?

ACKNOWLEDGMENTS

One of the authors (Y.T.) is thankful for the fruitful discussions he had with Dr. J. Fineberg, Dr. K. T. Coughlin, and Dr. R. Tagg. The authors also would like to thank Professor M. Maeda and Professor K. Hishida of Keio University for their continuing support and encouragement.

[1] P. R. Fenstermacher, H. L. Swinney, and J. P. Gollub, J. Fluid Mech. **94**, 103 (1979).
[2] P. S. Marcus, J. Fluid Mech. **146**, 65 (1984).
[3] M. Gorman and H. L. Swinney, J. Fluid Mech. **117**, 123 (1982).
[4] L. H. Zhang and H. L. Swinney, Phys. Rev. A **31**, 1006 (1985).
[5] K. T. Coughlin and P. S. Marcus, J. Fluid Mech. **234**, 1 (1992); **234**, 19 (1992).
[6] K. T. Coughlin, P. S. Marcus, R. P. Tagg, and H. L. Swinney, Phys. Rev. Lett. **66**, 1161 (1991).
[7] R. C. DiPrima and H. L. Swinney, in *Hydrodynamic Instabilities and the Transition to Turbulence,* edited by H. L. Swinney and J. P. Gollub, Topics in Applied Physics Vol. 45 (Springer-Verlag, Berlin, 1985).
[8] See, e.g., Y. Takeda, Nucl. Eng. Des. **126**, 277 (1991).
[9] Y. Takeda, W. E. Fischer, K. Kobashi, and T. Takeda, Exp. Fluids **13**, 199 (1992).
[10] H. A. Snyder, J. Fluid Mech. **35**, 273 (1969).
[11] Y. Takeda, K. Kobashi, and W. E. Fischer, Exp. Fluids **9**, 317 (1990).
[12] P. S. Shaw, C. D. Andereck, L. A. Reith, and H. L. Swinney, Phys. Rev. Lett. **48**, 1172 (1982).
[13] M. Gorman (private communication).
[14] Figure 6 of Ref. [3].